Mesoscopic Computational Haemodynamics

Artoli, A.M.M.

Publication date
2003

Chapter 4

Error Analysis for Steady Flow Simulations

In this chapter we perform three initial tests for the lattice Boltzmann method with BGK approximation. In all cases, steady flow simulations are investigated. The first two categories present and discuss results obtained from 2D simulations of the channel flow and the Couette flow benchmarks and study the error behaviour in velocity and shear stress. We study different boundary conditions and compare them for the two benchmarks. Machine accuracy is reproduced for the channel flow under certain conditions. The third category discusses simulation results performed on a symmetric bifurcation in a range of Reynolds numbers. The obtained simulation results are compared to a finite volume simulation for the same geometry under the same conditions, all showing excellent agreement.

4.1 Channel Flow

As a simple benchmark, channel flow between two fixed parallel plates separated by a distance h is investigated. If the flow is in the positive x-direction, the analytical solution for the channel flow is

$$u_x = \frac{4U_c}{h^2} y(h-y) \tag{4.1}$$

where y is the distance from the lower wall, $U_c = -\frac{1}{2\eta}\frac{dp}{dx} \equiv \frac{h^2 G}{8\rho\nu}$ is the centreline velocity derived by a pressure drop per unit length, dp/dx, or a body force G, and $\eta = \rho\nu$ is the fluid viscosity. The stress tensor components obtained by using Eq. (3.22) are to be compared with those defined by Eq.(2.15). The stress tensor components defined by Eq.(2.15) yield

$$\sigma_{xy} = \eta\frac{\partial u_x}{\partial y} = \frac{4\eta U_c}{h^2}(h-2y), \tag{4.2}$$

$$\sigma_{xx} = -p(x) \tag{4.3}$$

which is linear along the channel, and

$$\sigma_{yy} = -p(y) \tag{4.4}$$

which is constant across the channel. To verify our numerical model, we have carried out a number of simulations for the channel flow at $R_e = 10$ and $R_e = 90$. The system size $N_x \times N_y$ ranges from 20×10 lattice points for the coarsest grid to 100×50 for the finest grid. The system is initialised with zero velocity. The algorithm uses double precision to obtain the velocity profiles, the pressure and the stress tensor components, all being computed over the whole grid after the transients have died out. We have implemented two types of boundary conditions: the bounce-back rule for the walls and periodic boundary conditions in the horizontal direction, and the velocity boundary conditions (VBC) proposed by Zou and He (1997). For Poiseuille flow, since the centreline velocity is given by $U = \frac{h^2 G}{8\rho\nu} = \frac{R_e \nu}{h}$ (He et al., 1997), a uniform body force $G = 8\rho R_e \nu^2 / h^3$ along the x-direction is applied. The amplitude of this body force is changed with the grid resolution while keeping fixed both the Reynolds and the Mach numbers. He *et al.* (1997) analytically proved that the LBM has a solution for the velocity u_x for the channel flow, given by

$$u_x = \frac{4U_c}{n^2} y(n-y) + U_s, \tag{4.5}$$

where U_s is the slip velocity at the boundary. In the case of the bounce-back on the links, they claimed that the slip velocity is given by

$$U_s = \frac{2U_c}{3n^2}[(2\tau - 1)(4\tau - 3) - 3n] \tag{4.6}$$

where U_c is the centreline velocity without slips at the boundaries, $h = n\delta_x$ the width of the channel and n the number of nodes representing the width of the channel. The analytical solution for the shear stress in this case therefore becomes

$$\sigma_{xy} = \eta \frac{4U_c}{n^2}(n - 2y). \tag{4.7}$$

This equation is equal to the analytical solution of the shear stress for the channel flow (see Eq. (4.2)). This shows that with the bounce-back rule, the shear stress is not affected by the slip velocity, and therefore, it can be computed up to machine accuracy. For the shear stress, we have observed errors of the order of 10^{-15}, which is of the order of the roundoff error.

On the other hand, we have used the VBC proposed by Zou and He (1997) to implement a parabolic velocity profile at the inlet, a constant density at the outlet, and no slip conditions at the upper and the lower boundaries. On the boundaries, values for the distribution functions are computed at each time step from the imposed velocity or density and the known distribution functions streaming from the fluid to the boundary. The bounce-back scheme is assumed to be valid for the non-equilibrium

part of the particle distributions normal to the boundary. The densities at the corner points are assigned values from their nearest neighbouring fluid nodes. With VBC, the system is initialised with zero velocity components.

As mentioned before, the Kramer problem degrades the analytical solution near the boundary and the accuracy depends on the used boundary condition assigned at the obstacle. The simulation results are in good agreement with the expected theory when VBC is used, but obtaining machine accuracy has not been possible with the standard lattice BGK model. This is due to the influence of compressibility errors. We will present the error analysis for the shear stress in the channel flow together with the error analysis for the shear stress in the Couette flow problem in section 4.3.

4.2 Plane Couette Flow

We have selected this benchmark as a simple example of a two-component flow which has an exact analytical solution but is not an exact solution of the lattice BGK equations (He *et al.*, 1997). For the Couette flow with vertical injection at the upper and the lower boundaries, we consider the lower wall to be fixed while the upper wall moves along the horizontal direction with velocity u_n. The vertical injection speed is assumed to be $u_y = constant$. The two plates are separated a distance h. Since the lower wall is fixed, the analytical solution for the horizontal fluid velocity is (He *et al.*, 1997)

$$u_x = \frac{exp\left(\frac{R_e}{h}y\right) - 1}{exp(R_e) - 1} u_n \tag{4.8}$$

where the Reynolds number is defined as $R_e = u_y h/\nu$. Consequently, the analytical solution for the shear stress component is

$$\sigma_{xy} = A\ exp\left(\frac{R_e}{h}y\right), \tag{4.9}$$

where $A = \frac{\eta u_n R_e}{h(exp(R_e)-1)}$ is the value of the shear stress at the lower boundary. The other two components of the stress tensor are

$$\sigma_{xx} = -p(x) \tag{4.10}$$

which is constant along the channel when using periodic boundary conditions, and

$$\sigma_{yy} = -p(y) \tag{4.11}$$

which is also constant across the channel.

The analytical lattice BGK solution for the Couette flow with injection is (He *et al.*, 1997)

$$u_x = \frac{\lambda^j - 1}{\lambda^n - 1}(u_n + U_s^n) + \frac{\lambda^n - \lambda^j}{\lambda^n - 1}(u_0 + U_s^0) \tag{4.12}$$

where $\lambda = (2+R)/(2-R)$ with $R = u_y\delta_x/\nu$, u_0 is the velocity of the bottom wall ($u_0 = 0$ in our case), U_s^n and U_s^0 are the slip velocities at the top and the bottom walls, respectively. This solution is a second order approximation for the Navier-Stokes analytical solution given by Eq. (4.8). If the shear stress is computed from the derivative of this velocity, it yields

$$\sigma_{xy} = B\lambda^j \tag{4.13}$$

where

$$B = \frac{\eta ln(\lambda)}{\lambda^n - 1}\left[(u_n + u_0) - (U_s^0 + U_s^n)\right] \tag{4.14}$$

In our case, as the bottom wall is fixed, while using the no-slip VBC are used, B will have the simple form

$$B = \frac{\eta ln(\lambda)}{\lambda^n - 1}u_n \tag{4.15}$$

which is equal to A in Eq. (4.9) when we replace the Reynolds number R_e with $R_e^* = n\,ln(\lambda)$. The difference between the two Reynolds numbers reflects the finite difference errors.

The first order behaviour has also been studied in the case of the Couette flow problem, by assigning the equilibrium distributions to the distribution functions at the walls and periodic boundaries in the x-direction. With the equilibrium distribution boundary conditions, the slip velocities have the analytical lattice BGK forms (He *et al.*, 1997)

$$U_s^0 = -\frac{(\tau-1)(\lambda-1)(\tau\lambda-\tau-\lambda)}{\lambda^n(\tau\lambda-\tau+1)+\lambda(\tau\lambda-\tau-\lambda)}(u_n - u_0), \tag{4.16}$$

and

$$U_s^n = \frac{(\tau-1)(\lambda-1)\lambda^n(\tau\lambda-\tau+1)}{\lambda^n(\tau\lambda-\tau+1)+\lambda(\tau\lambda-\tau-\lambda)}(u_n - u_0), \tag{4.17}$$

which are of first order in space. The initial value of the shear stress in this case can be obtained by substituting Eqs. (4.16) and (4.17) into Eq. (4.15). It can be proved that as $\delta_x \to 0$, the slip values of the shear stress at both walls are proportional to $1/n$.

Hence, we have three formulae for computing the shear stress:

- from the analytical Navier-Stokes solution, as given by Eq. (4.9),
- from the analytical lattice BGK solution, as given by Eq. (4.13), and
- directly from the non-equilibrium parts of the distribution functions, as given by Eq. (3.22).

To compare these methods, we have carried out numerical simulations for this Couette flow problem at $R_e = 10$. The size and the initial state of the system are the same as those described previously for the channel flow problem. For the boundaries, we have first implemented the VBC for the upper and the lower boundaries and periodic

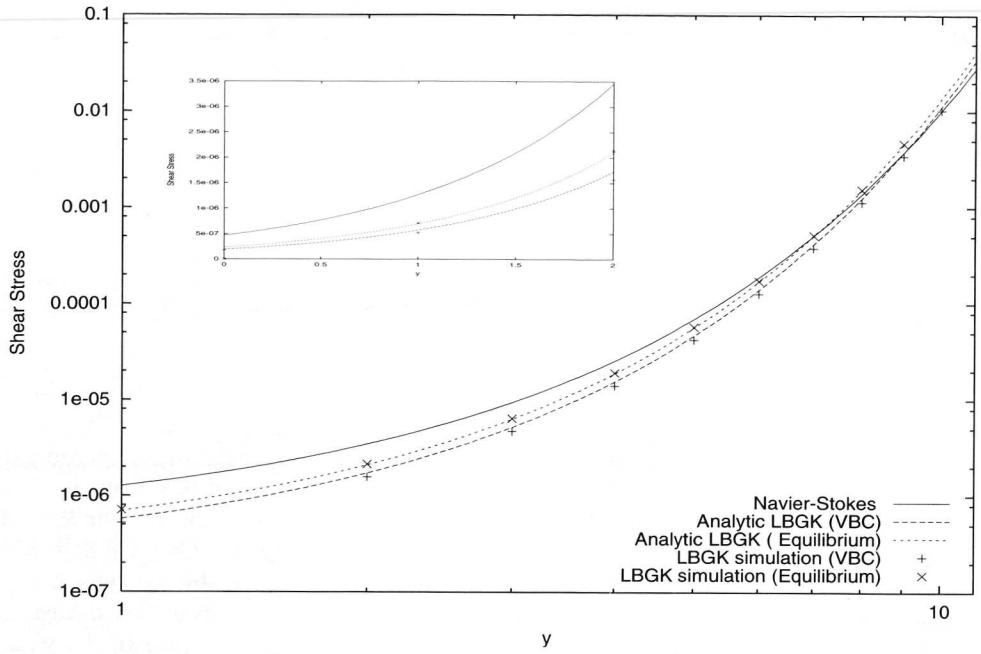

Figure 4.1: Shear stress computed from the distribution functions (Eq. (3.22)) compared to that computed from the Navier-Stokes solution (Eq. 4.9) and the derived lattice BGK analytical solutions (Eq. 4.13), using VBC and equilibrium distributions, for $R_e = 10$, in the Couette flow benchmark. Values at $y = 0$ are zoomed inside the figure.

boundaries in the horizontal directions. We have also performed a similar simulation for the Couette flow problem using the equilibrium distributions at the boundaries and periodic boundaries in the x-direction. In each case, good agreements with analytical solutions have been obtained, as can be seen from Fig. 4.1, from which we also notice that the equilibrium distributions yield zero values for the shear stress at the boundaries. This is attributed to the fact that $f_i^{(1)} = 0$, and may be maintained by using Eq. (4.13) or extrapolating from the nearest points. We are interested in the equilibrium distributions because they are easy to use for non-uniform inlet and outlet boundaries (see Chapter 8).

4.3 Error Analysis

Although these two benchmarks have been classically investigated by many authors, here we find it necessary to test the accuracy of the used algorithmand investigate

the accuracy of the stress tensor for these simple benchmarks.
We have carried out a number of simulations with different grid sizes at constant values of the relaxation parameter τ at various Reynolds numbers in the range 1–100 for both the channel flow and the Couette flow with injection. The measured error Ev in the velocity is calculated using the formula

$$Ev = \frac{\sum_{x,y} |u_x - u_x^*|}{\sum_{x,y} |u_x^*|} \tag{4.18}$$

where u_x^* is the analytical solution for the velocity at the given grid location and the summations are taken over the whole grid. Similarly, the error Es in the shear stress component is computed from

$$Es = \frac{\sum_{x,y} |\sigma_{xy} - \sigma_{xy}^*|}{\sum_{x,y} |\sigma_{xy}^*|} \tag{4.19}$$

where σ_{xy}^* is the analytical solution for the shear stress component at the given grid location. While using the VBC, the error behaviour for the channel flow and the Couette flow with injection at the boundaries is shown in Fig. 4.2 for $R_e = 10$. For $R_e = 10$, the slopes of the lines are -2.0 for the channel flow and -1.8 for the Couette flow with injection. Similar results have been obtained for $R_e = 90$, where the slopes are -2.0 for the channel flow and -1.7 for the Couette flow with injection. From this figure, we observe that the error in the shear stress behaves the same as the error in the velocity fields, which is a second order error for the VBC. Moreover, the error in the shear stress is approximately of the same magnitude as that of the velocity, as predicted from theory. However, we have obtained machine accuracy with the incompressible D2Q9i model proposed by Zou *et al.*(1995).

Since the Reynolds number is a critical parameter in the case of the Couette flow with injection, we have carried out a number of simulations with $R_e = 6$, $R_e = 30$ and $R_e = 60$ at $\tau = 1$ for this benchmark. The results are shown in Fig. 4.3. For the shear stress, the slopes are approximately -1.9 for the three Reynolds numbers. However, the order of the error increases with the Reynolds number and more grid refinement is needed to recover the same accuracy. For $R_e = 30$ and $R_e = 60$, the grid is respectively 25 and 100 times larger than the case for $R_e = 6$.

Using the bounce-back rule for the channel flow, we have observed errors of the order of 10^{-15} for the stress tensor while a first order error has been obtained in the velocity. The error in the velocity in this case is attributed to the slip velocity which can be subtracted to yield the same order as the shear stress. This shows that, with the simple bounce-back rule, the shear stress yields perfect agreement with the analytical solutions. This result has a direct impact on haemodynamics, as will be realised later.

For the Couette flow benchmark, while assigning the distribution functions their corresponding equilibrium distributions at the walls and periodic boundaries in the x-direction, the error in the shear stress is of first order. However, as shown in Fig. 4.1,

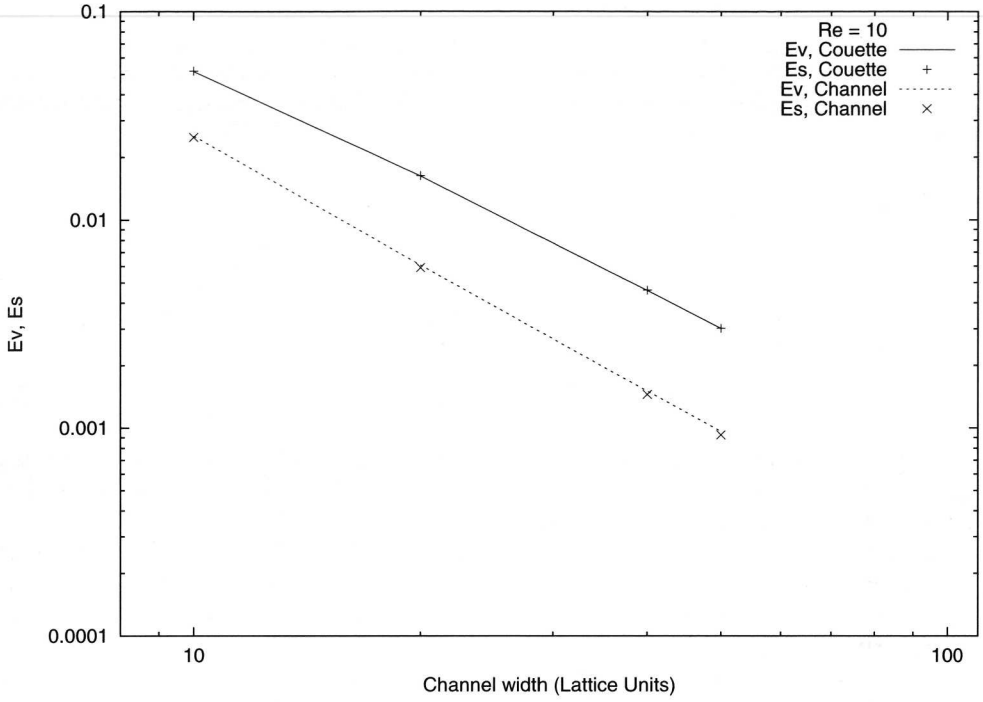

Figure 4.2: Relative errors in v_x and σ_{xy}, using the LBM with the velocity boundary conditions for $R_e = 10$, in the channel and the Couette flows.

the shear stress obtained by using equilibrium distributions is not different from the shear stress computed from the derivative of the analytical lattice BGK solution for the velocity, except at the boundary nodes where the theory fails. It is also clear from the figure that with the equilibrium distributions, the shear stress inside the flow domain has values closer to the shear stress derived from the analytical Navier-Stokes solution for the velocity than values obtained by the second order VBC. This may be attributed to the fact that VBC are derived by assuming that the bounce-back is valid for the non-equilibrium parts of the distribution function, from which the shear stress is computed.

4.4 Convergence Behaviour

As assumed by the Boltzmann equation, approach towards equilibrium shall be guaranteed when the Boltzmann equation is correctly solved by any means. Figure 4.4 shows the error magnitude as the simulation creeps towards its Maxwellian equilibrium with different lattice sizes. It is to be noticed that, at the beginning, coarse grids may be more accurate than finer ones. The reason for this is that the number

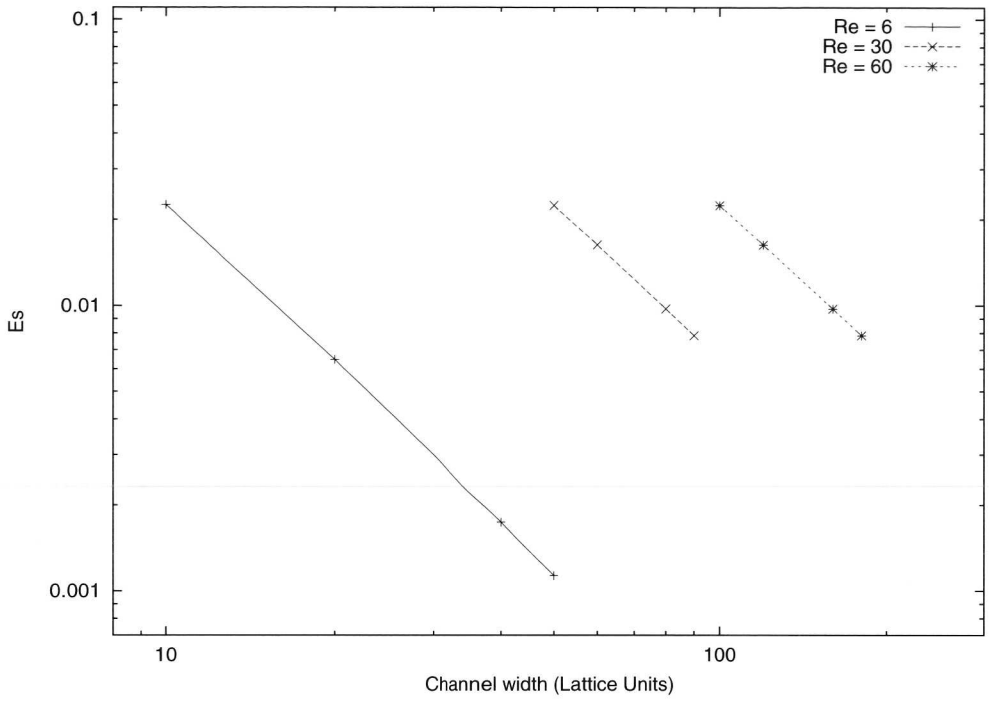

Figure 4.3: Relative errors in σ_{xy}, using the LBM with the velocity boundary conditions, for $R_e = 6, 30$ and 60 , in the Couette flow benchmark.

of unknowns increases with the number of nodes[1], and therefore the system needs more simulation time before it updates all the nodes of the fine grids, at the right edge of the figure. For interactive or real-time simulations, coarse grids may therefore be preferable than fine ones, unless certain small-scale flow characteristics are of interest. However, there is a minimum number of grid points that allows a stable solution. This depends strongly on the compressibility error which increases with δ_x and the Reynolds number.

4.5 The Symmetric Bifurcation

We are interested in the symmetric bifurcation as a more complex two-dimensional benchmark to investigate the accuracy of the shear stress in the LBM. This benchmark will be used later as an investigative benchmark for interactivity and robustness of the lattice Boltzmann method (see Chapter 7).
As we mentioned before, there is a direct relation between the shear stress and

[1]This is similar to real fluid streaming behaviour.

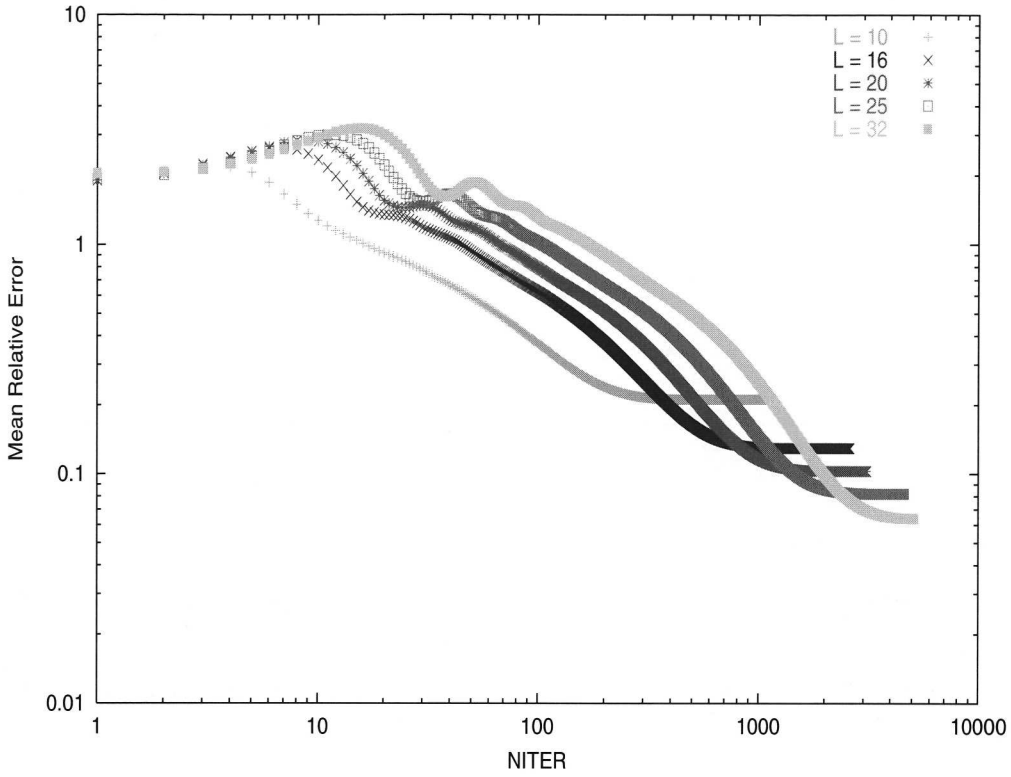

Figure 4.4: Temporal error behaviour in the Couette flow problem.

Atherosclerosis, which is a highly localised disease in areas of the carotid, coronary and femoral arteries and abdominal aorta. All these locations have complex geometry, such as branching and bifurcation, complex flow patterns, secondary flow and complex shear stress.

Several numerical and experimental models of fluid flow in large arteries and bifurcating tubes have been extensively studied (e.g. Friedmann *et al.*, 1974, Ojha, 1994;Qiu and Tarbell, 2000). However, in these attempts, the use of the derivatives of the velocity fields to get the shear stress was quite common. Within the LBM community, this benchmark did not receive much attention. This may be attributed to three reasons. Firstly, the analytical solution for the symmetric bifurcation is not known. Secondly, it is not easy to implement accurate and flexible boundary conditions at the outlets. Finally, this application is a good benchmark in biomechanics and the lattice Boltzmann method is just recently being used in this field. However, studying the

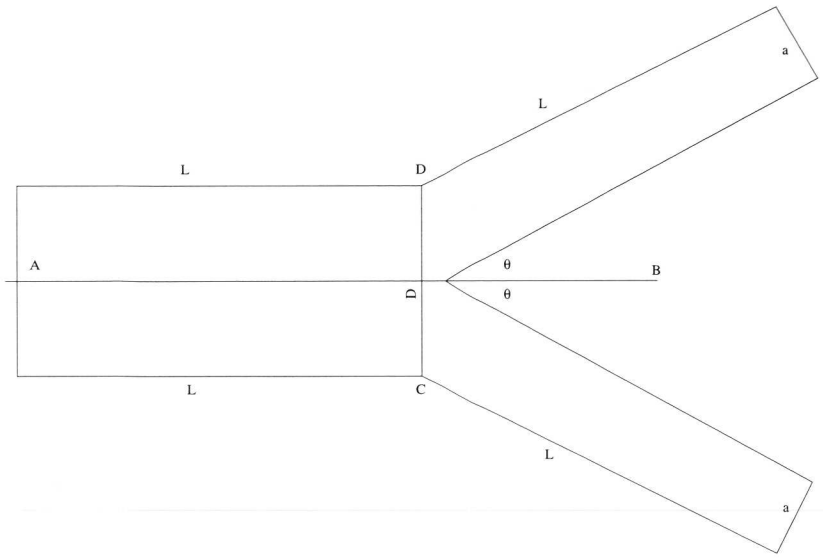

Figure 4.5: Geometry of the simulated symmetric bifurcation

symmetric bifurcation as a benchmark for blood flow problems gives us a clearer idea about the complexity of the flow field and the shear stresses at locations of interest. Additionally, it allows us to investigate implementation of several boundary conditions before using them for more complex geometry.

In this study, we consider a simplified model of a two-dimensional symmetric bifurcation that consists of one main tube of diameter D and length L and two branches at the end of the main tube, each of which has an outer length L and diameter $a = D/2$. The angle θ between each branch and the centerline AB that passes horizontally across the divider is set to be equal to 30^o. The geometry of the symmetric bifurcation is illustrated in Fig. 4.5 in which the centerline AB and the cross line CD will be reference axes for measurements and comparisons of the flow fields and the components of the stress tensor.

It can be shown that the cross sectional area of this two-dimensional bifurcation model does not change, as long as $a = D/2$. Using this result and applying the continuity equation to the model, we can prove that the average velocity in the main branch is equivalent to the average velocity in the daughter branches. This allows us to impose consistent velocity values at the inlet and outlet boundaries. On the other hand, the pressure gradient in the branches can be compared to that in the main branch by assuming that the Poiseuille formula still holds in regions far from the divider region and applying the continuity equation to end up with the conclusion that the pressure gradient in the branches is four times larger than the pressure

drop in the main branch. Assuming that the Poiseuille formula is still valid for locations of fully developed flow in the bifurcation, the shear stress in these areas will not differ significantly from values obtained from a similar channel flow. Therefore, the only region which needs further investigation is the region close to the divider. The geometry of the symmetric bifurcation whose vascular area does not change, makes the region just before the divider an expanding region. This additional area has to be filled by the fluid. As a result, both the pressure and the velocity will drop near to the divider before they enter the branches, where the velocity accelerates towards the fully developed flow and the pressure drops faster than the pressure in the main branch.

In order to obtain a more quantitative picture of the flow, we have carried out a number of LBM numerical simulations for the symmetric bifurcation at $R_e = 1$, $R_e = 200$ and $R_e = 1250$, where $R_e = DU_0/\nu$ is the Reynolds number. The diameter of the main branch is represented by 40 lattice points on the coarsest grid and 320 lattice points on the finest grid. At the inlet, we have set a flat velocity U_0 of magnitude corresponding to the required Reynolds number. The distribution functions and the density at the inlet are computed using the VBC, as described before. For the outlets, we have assumed that the flow is fully developed at a distance far from the divider by setting parabolic profiles at each outlet and forcing the distribution functions to their equilibrium values. Finally, for the other walls, we have implemented the simple bounce-back scheme.

For validation purposes, we have used the FLUENT program (Fluent, 1998) which uses a finite volume method (FVM) solver, to carry out a number of simulations for the same bifurcation at the three Reynolds numbers[1]. The comparison is made along the centerline AB and the cross line CD.

The velocity profiles and the shear stress as obtained by LBM are shown in Figs. 4.6 (a–f) for the three Reynolds numbers. As shown from these figures, the flow field fully develops just after the inlet region for $R_e = 1$. However, for the larger Reynolds numbers, the flow field is not yet fully developed when entering the divider region. At the outlets, the flow is fully developed (as we assumed) for $R_e = 1$ and $R_e = 200$. For $R_e = 1250$, it appears that the flow is not fully developed at the outlets, but this doesn't have significant effects on the flow closer to the divider (experiments of varying lengths of the branches didn't show significant difference (data not shown)) . It can also be observed that the flow near the divider becomes complex. As the region before the divider is an expansion region, the velocity flow pattern drops before entering the branches. We also observe that the velocity skews towards the inner walls inside the daughter branches and each of the two streams are bent because of the influence of the secondary motion, with the highest velocities near the outer walls of the bend. All these features are in agreement with the literature (Caro *et al.*, 1978;

[1]The finite volume simulations were carried out in collaboration with Huub Hoefsloot. See Artoli *et al.*, 2003d

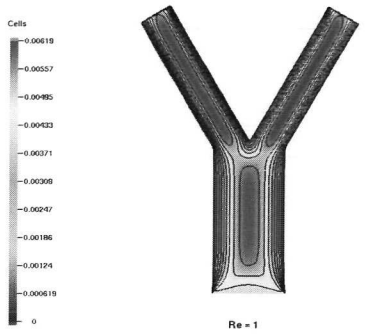

(a)

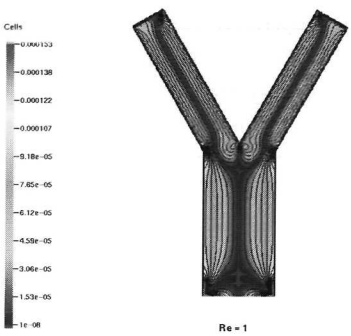

(b)

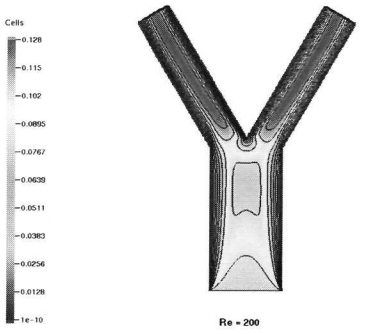

(c)

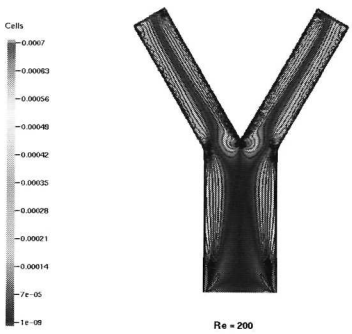

(d)

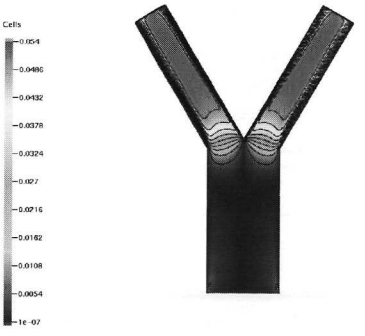

(e)

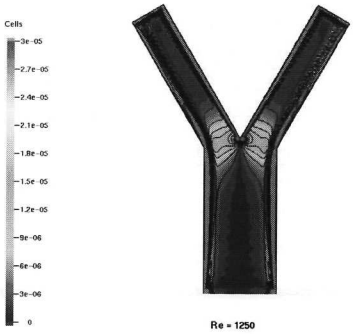

(f)

Figure 4.6: Contours of velocity magnitudes and shear stress in Lattice Units for $R_e = 1(dx/dt = 0.0091$ m/sec), $R_e = 200(dx/dt = 0.0912m/sec)$ and $R_e = 1250(dx/dt = 0.5706m/sec)$.

Berger and Jou, 2000) and with the solutions of the FVM results.

The σ_{xy} components at the inlet are very close to zero, because of the imposed flat velocity profile. The corner points C and D and the divider region show higher stress values. The stress in the inner walls of the daughter branches is larger than that at the outer walls. As the Reynolds number increases, the shear stress behaves more complex, especially around the divider.

Next, results obtained from the LBM are compared to those obtained by the FVM, by taking measurements along the cross line CD. Acceptable agreement between the results obtained from the LBM and the results obtained from the FVM has been achieved when comparing the two components of the velocity (Figs. 4.7 (a–c) for v_x and (d) for v_y). The two methods show that the maxima of v_x are shifted towards the outer walls before entering the expansion region and these maxima approach the wall as the Reynolds number increases (since the velocity component increases). As it is shown in Fig. 4.7 (a) for $R_e = 1$, the maximum difference in the x-component of the velocity occurs at the centre point which faces the divider for $R_e = 1$. This is because of the flexibility of the finite volume method in performing local grid refinements at complex regions. For $R_e = 200$ and $R_e = 1250$, the differences are less than one percent. We also observe that the LBM solution approaches the FVM solution as the grid refines (see e.g. Fig. 4.7 (a)).

The stress tensor component, σ_{xy}, shows good agreement for both methods, as is shown in Figs. 4.7 (e–g) for the three Reynolds numbers. We can observe that σ_{xy} becomes quite complex in the case of $R_e = 1250$, where the shear stress changes sign more frequently. It is worth noting that the bounce back rule yields good results for the shear stress close to the wall, since it is not affected by the slip velocity. On the other hand, assigning the equilibrium distributions at the outlets yields completely wrong values of the stress tensor near to the wall. This is clearly seen from the contour lines of the shear stress at the outlets, specially for $R_e = 1$.

While looking at the results along the centerline AB, we have observed good agreement between the two numerical methods for v_x (data not shown). However, discrepancy in the pressure drops has been observed for small Reynolds numbers. The maximum difference between the two solutions is about 20% , which occurs at low Reynolds number, near to the divider. This may be attributed to the minor artifacts in the lattice BGK approximation and can be eliminated by considering generalised models.
For the stress tensor components along the centerline, the off-diagonal components, σ_{xy} has zero values far from the divider in both the LBM and the FVM. Since $\frac{\partial v_y}{\partial y} = 0$ on the line AB, it turns out that $\sigma_{yy} = -p$ (see Eqs. 4 and 5). This presents a good consistency check for LBM. In Fig. 4.7(h) we compare σ_{yy}, calculated by Eq. (3.22), with $-p = -\rho c_s^2$, for the three Reynolds numbers. In all cases, good agreement is observed.

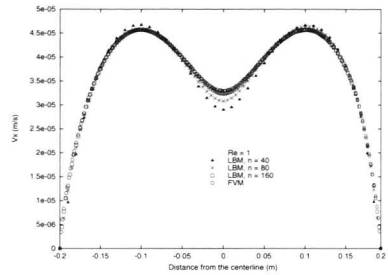

(a)

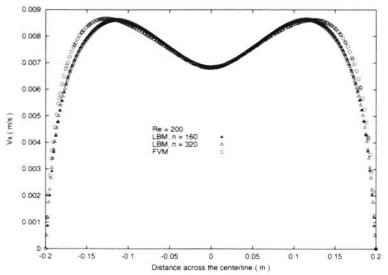

(b)

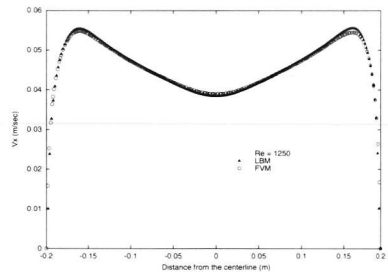

(c)

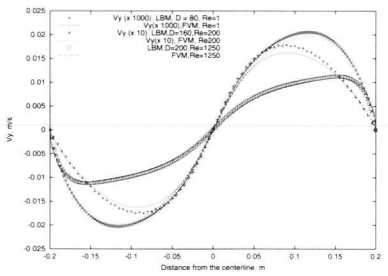

(d)

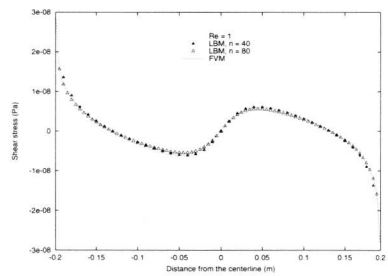

(e)

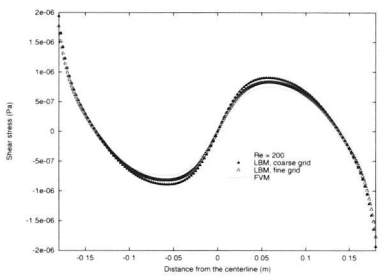

(f)

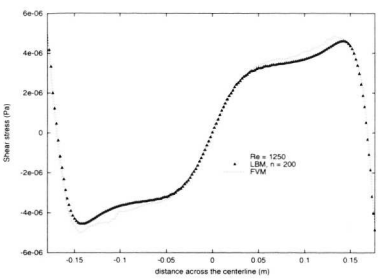

(g)

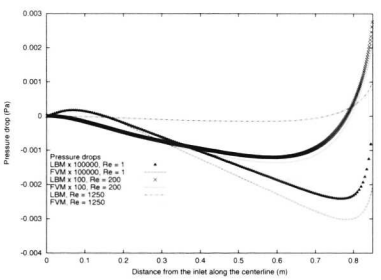

(h)

Figure 4.7: Comparison of LBM velocity profiles (upper four graphs) and shear stresses (lower left) with the FVM solution along the line CD of the symmetric bifurcation for $R_e = 1$, 200 and 1250 with different grid resolutions. The lower right graph shows the pressure drop along the centerline AB.

From this experiment we conclude that although the flow near the divider of a symmetric bifurcation is complex, we can obtain results of comparable accuracy to the finite volume method, by computing the stress tensor components from the non-equilibrium parts of the distribution functions, commonly computed during the collision process of the lattice BGK simulations.

4.6 Summary

Three independent 2D numerical simulations have been used to validate the lattice BGK for simple steady flows: the channel flow, the Couette flow with injection at the boundaries and the symmetric bifurcation. We have implemented a number of boundary conditions known to the LBM community. We have also shown that the accuracy of obtaining the stress tensor from the LBM follows the accuracy of the implemented boundary condition, except for the bounce-back rule, where the error is of the order of the machine accuracy in the case of channel flow. We have also compared the obtained results with the analytical solutions derived from the analytical lattice BGK solution for the velocity field which has been obtained by He *et al.* (1997) and the Navier-Stokes solution for the shear stress in the Couette flow with injection. In the case of the symmetric bifurcation, the results are comparable to the FVM results. It has been shown that, close to the walls, the wall shear stress can be computed with high accuracy using the lattice BGK. The method proved to be successful in computing the stress tensor in complex geometry, in the limit of low Mach number. As there is an increasing interest in applying the LBM in haemodynamics, we argue that similar formula for the stress tensor for non-Newtonian fluids may be worked out. Further experimental and simulation studies on 3D flows are necessary for validation and more enhanced boundary conditions for the outlets may be required. These issues will be discussed in the next chapter.